NASA Technical Paper 3235

1992

Track Structure Model of Cell Damage in Space Flight

Robert Katz
University of Nebraska
Lincoln, Nebraska

Francis A. Cucinotta,
John W. Wilson,
and Judy L. Shinn
Langley Research Center
Hampton, Virginia

Duc M. Ngo
Old Dominion University
Norfolk, Virginia

NASA
National Aeronautics and Space Administration
Office of Management
Scientific and Technical Information Program

1. Summary

Cell damage by high linear energy transfer (LET) radiations has been described by a phenomenological model (track theory) for more than 20 years. With track theory, molecules of biological significance (dry enzymes and viruses) act as one-hit detectors. Recent additions to the class of one-hit detectors are *Escherichia coli B*, and single- and double-strand breaks in SV-40 virus in EO buffer, where indirect effects predominate. The response of cells (survival, transformation, and chromosome aberration) to these radiations is typically described by a four-parameter model whose numerical values are determined from the equations of the theory being fit to experimental data at high dose (typically above 1 Gy), with the cells bombarded by gamma rays and high-charge-and-energy (HZE) particle beams, of the widest possible dynamic range. Once these parameters are determined, the model predicts cellular response in any radiation environment for which the particle-energy spectrum is known. The important feature of this track structure model is its ability to estimate from a limited set of laboratory data the response of a complex radiation environment with many components. For example, we have calculated cell survival after neutron irradiation with mixtures of neutrons and gamma rays and cell survival and transformation after irradiation with HZE of different energies. The model does not yet include cellular repair, although some hopeful approaches to repair dependence are now being developed. It also does not include cancer induction because the available data give neither the number of cells at risk nor the number of cancers induced and are thus not suited to our formulation.

Most recently, NASA Langley models of HZE beams, including projectile and target fragmentation types, have been joined with the track structure model. This combination has been tested with good success against ground-based radiobiological data for cell survival after irradiation with protons and HZE beams. And whereas our earlier beam model failed downstream of the Bragg peak (for both protons and heavy ions) for want of a proper description of fragmentation, the current model succeeds.

Based on this experimental validation of our procedures, we have initiated calculations of cellular damage in spaceflight from solar protons and galactic cosmic rays. In this paper we incorporate NASA Langley models of cosmic rays, beam penetration, and projectile and target fragmentation with track theory. The essential radiobiological theme is that knowledge of parameters found at high doses enables us to calculate the response of cells at the lowest possible doses of HZE particles when only intratrack (ion-kill) effects are involved. Our procedures here too have ground-based experimental validation, wherein measurements made with protons and alphas of relative biological effectiveness (RBE) of the survival of C3H10T½ cells, at doses down to 0.01 Gy, were consistent with our predictions that were based on survival measurements made at high doses with gamma rays and HZE's.

2. Introduction

Detectors of radiation differ according to whether single-particle response is normally observed, as with nuclear emulsions, solid-state nuclear track detectors, and scintillation counters, or whether the response is to beams of particles or photons in a gross macroscopic irradiation, as in radiobiology or in the alteration of bulk material properties by radiation. In the former case it is more natural to think in terms of track structure, whereas in the latter case one frequently refers to macroscopic dose (Katz 1978b). Response is then correlated to the physical description of these stimuli. It is common to relate response to energy deposition (dose). Problems arise because response depends not only on total energy deposition but also on the microscopic structure of that deposition and its time development. One analysis of these details is called *microdosimetry*, the study of energy deposition in small volumes, which stimulated many investigations. An alternate procedure favored in this paper relates the observed effect to track structure for individual particles, and the effect then may be related to macroscopic dose for gross irradiations. These perspectives are principally reported in the several Symposia on Microdosimetry sponsored by the Commission of European Communities (Katz and Huang 1991; Katz, Dunn, and Sinclair 1985).

The galactic cosmic ray (GCR) environment is the most complicated mixture of radiation components known. It is doubtful that the GCR environment will ever be adequately simulated in the laboratory for biological experiments. The primary role of track-structure models will be to extrapolate laboratory response data to the GCR environment for the estimation of risk to biological tissues in space exposure. We believe this extrapolation will be a more practical approach to the problem of additivity of response of disparate components than the usual quality-factor approach based on relative biological effectiveness (RBE), which has been used with limited success in terrestrial radiation protection.

This paper is organized as follows: We first discuss several of the approaches for describing

radiation insult and emphasize the question of additivity of radiation components. The track-structure model and its mathematical formalism are then described. The Langley models of high-charge-and-energy (HZE) transport are compared with cell survival experiments and predictions of cell damage in space flight from galactic cosmic rays are discussed. Finally, significant conclusions are given.

Research at the University of Nebraska is supported by the U.S. Department of Energy.

3. Symbols and Abbreviations

A	mass number
a_0	sensitive site radius, cm
C	hittedness
D	absorbed dose, Gy
$\overline{D}$	average radial dose, Gy
D_x	X-ray dose, Gy
D_γ	gamma-ray dose, Gy
E	energy, MeV
E_0	radiosensitivity parameter, Gy
E_{0_j}	average energy of fragment j, MeV
F	fluence, cm^2
f	secondary ion spectrum, MeV^{-1}
G	number of observed events per unit of energy deposited
GCR	galactic cosmic ray
HZE	high charge and energy
L	stopping power, MeV/cm
LET	linear energy transfer, MeV/cm
m	target number
N	cell population after exposure
N_0	initial cell population
n	number of observable events per centimeter of path length
P	ion-kill probability
p	proton
QF	quality factor
RBE	relative biological effectiveness
RBE_{ext}	extrapolated relative biological effectiveness
S	target cross section, cm^2
S_0	plateau value of the target cross section
TLD	thermoluminance detector
t	radial distance, cm
x	position, cm
Z	charge number
Z^*	effective charge number
β	relative particle velocity
κ	track structure parameter
Π_i	ion-kill fraction
Π_γ	gamma-kill fraction
Σ	macroscopic nuclear interaction cross section, cm^{-1}
σ	action cross section, cm^2
σ_{ext}	extrapolated action cross section, cm^2
σ_0	plateau value of action cross section, cm^2
σ^*	effective action cross section, cm^2
τ	mission duration, yr
Φ	particle flux spectrum, #/MeV-cm^2-s

Subscripts:

j	fragment label
n	neutron

4. Concepts From Radiobiology

4.1 Microdosimetry: Energy Deposition in Small Volumes

One way to analyze stimuli to biological systems is to examine the details of energy deposition in small volumes that are sized to represent what are thought to be critical targets within the cell. Experimentally small, gaseous proportional counters are used whose diameters, scaled to the density of tissue, range from micrometers to nanometers in unit-density material. The critical targets are then considered to be the nucleus of a mammalian cell, a chromosome, or a small region of DNA. The fluctuations of the energy deposited within the small target region are assumed to be related to biological response. A Monte Carlo simulation of a radiation field can yield a similar decomposition.

Even when one has a complete microdosimetric description of the radiation environment, the problem remains as to how that description may be interpreted to predict the response of a detector. As yet we have no means of calibrating response in terms of the statistical distribution of energy depositions in small volumes; nor do we know what volume is appropriate. It is on this level that microdosimetry has not been able to make extensive quantitative predictions, nor has it been able to yield calculations of cross section. But microdosimetry has yielded many interesting insights into the structure of a radiation field. (See, for example, Goodhead 1988.) The small counter has found applications in monitoring neutron beams that are used in radiotherapy and in other radiation fields, including spacecraft and high-altitude aircraft. Most instruments are used in practice to derive averages over quality factors discussed in section 2.5.

4.2 Cross Section

A second approach to analyze stimuli to biological systems is to attempt to mimic the kind of logical structure that is used in experiments in physics, that is, to describe the relevant interactions through the concept of an interactive cross section. We imagine that a projectile passing down a channel 1 cm^2 in area interacts with a target located somewhere within that channel, and we then measure the fraction of successes after a large number of identical repeated trials. The probability of success is represented as though it is a geometrical target, as the cross section σ in square centimeters to the cross-sectional area of the channel. We then speak of the *action* cross section even if the observed end point is achieved as a result of many internal changes stimulated by the initial interaction. We make no attempt to examine the internal processes mechanistically: the target is a black box. We know only the incident radiation and the observed end point. In radiobiology the concept of action cross section is sometimes used in ways that depart from its original physical meaning. This difference can lead to misinterpretations of experimental data (Katz 1990). Curtis et al. (1992) have recommended an additivity formalism based on a limited set of data for harderian gland tumorigenesis by using a cross-section-like formalism as an alternative to the use of RBE.

4.3 *G*-Value

When a projectile impinges on a thin slice of matter containing N_0 targets per cubic centimeter, the number of observable events per centimeter of path length is $n = \sigma N$. (If the stopping power is L, the number of observed events per unit of energy deposited, the G-value, is $G = n/L = \sigma N/L$. The cross section is a function of the medium, the end point, and the character of the projectile as follows: if a photon its energy, if a naked charged particle its charge and speed, and if a nucleus partially clothed with electrons its effective charge and speed. This formulation of the G-value has been used in the analysis of heavy ion radiolysis (Katz and Huang 1989). In dealing with liquids, where the meaning of N may be obscure, we have calculated the G-value for heavy ion bombardment from calculated values of the RBE and known G-values for gamma irradiation, as in the Fricke dosimeter (Katz, Sinclair, and Waligorski 1986). In other cases we have tried to relate N to a fitted target size. Nuclear collisions are here neglected except as a source of charged fragments.

If the G-value is normalized to molecular weight and expressed as events per radian per dalton rather than as events per 100 eV, we find it proportional to the RBE for dry one-hit detectors for which the target molecular weight is equal to the true molecular weight (Katz 1991).

4.4 Relative Biological Effectiveness and Radiation Quality Factor

When intense neutron environments became available for study, the existing body of biological response data was mainly for X-ray and gamma-ray sources. The first efforts at protection attempted to scale the known X-ray and gamma-ray risks according to equivalent neutron dose, and this scaling gave rise to the concepts of RBE and radiation quality. For the case of space radiations, we should like to relate the response of our detectors to energetic heavy ions (high LET radiations) to their response to photons and electrons (low LET radiations). In radiobiology the ratio of the dose of gamma rays to that of another radiation that produced the same observed end point is called the *relative biological effectiveness* (RBE). In radiotherapy this quantity is frequently taken to be a property of the two radiation fields, but it depends on the dose level, the dose rate, and the end point as well. An extension of this idea used in radiation protection is called the *quality factor* (QF), which is an estimate of the upper limit of RBE values for a selected set of biological end points judged relevant to human risk and taken solely as a function of LET. An important, unresolved question is whether an upper limit or maximum RBE is achieved at the low exposures of interest for radiation protection. The QF is used to convert a measured dose in gray into an effective dose reported (not measured)

in sieverts. A quantity in sieverts is not directly measurable and thus violates the underlying philosophy through which physical units are defined. The redeeming quality of the sievert is that risk estimates based on the unit should be conservative, providing QF is adequately defined. The conservative nature of the method may also be an unacceptable burden in many operations, especially in space where it may result in severe penalties in the form of substantial increases in shielding.

4.5 Radiation Dose and Quality

An irradiation with photons leads to secondary electrons randomly dispersed through a medium. The initial energy spectrum of these electrons and their path lengths depend on the initial energy spectrum of the photons. An irradiation with a beam of heavy ions yields a random distribution of heavy ion paths, with the secondary electrons (delta rays) clustered around each ion's path (correlation effects) and having a different energy distribution. Hence the delta rays are not truly randomly distributed, but are clustered about the paths of heavy ions. The difference in the spectrum of secondary electrons from photons and ions leads to a basic difference in the manner in which their effects are approached statistically. In the track structure model, *gamma kill* describes the effects of a random distribution of spatially uncorrelated electrons, and *ion kill* describes the effects of spatial correlations within single-particle tracks. At high fluences of low LET ions, where only a fraction of the intersected targets is inactivated, we attribute the effect of the sparsely distributed and overlapping delta rays from several ions to randomly distributed electrons and consider gamma kill to be responsible for part of the effect from beams of some heavy ions.

During irradiation with photons, minutes may elapse before secondary electrons traverse from different photons through a target (uncorrelated temporal events). During irradiation with heavy ions, however, a single ion and its delta rays pass through a target in an extremely short time because the projectile moves at nearly the speed of light through a target whose diameter is on the order of 1 μm. These differences in time separation lead to a variation in target response to radiations of different admixtures of photons and heavy ions at the same dose. When the temporal correlation time is on the order of the cell repair time, then response also varies with dose rate or fractionation schedule. The dependence on dose rate or fractionation schedule is due in part to radiation quality. The QF is taken as the low-dose rate limit of RBE's in an attempt to normalize the biological effects of radiations of different qualities. Choosing the quality factor in this manner thus assumes that it is logical to represent the response of a detector as a product of two separate factors, dose and quality.

4.6 Radial Dose Distribution

To make track-structure calculations, we need to determine the radial distribution of dose, from delta rays and the primary interactions, about the path of an energetic charged particle (Waligórski, Hamm, and Katz 1986). We presently use an analytic representation of the results of a Monte Carlo calculation made for liquid water for this purpose. More recently we have extended this model to include some solids used as radiation detectors (Katz et al. 1990). Additional information about both theoretical and experimental determinations of the radial dose distribution may be found in Katz and Varma (1991). We use this information in connection with the response of the detector to gamma rays to find the radial distribution of effect around a particle's path. Because we interpret the response as the probability for activating a target, we can make a map of the radial distribution of activated targets. If, for example, we are interested in the opacity of a track in nuclear emulsion, we can calculate the attenuation of a beam of light in a microscope photometer, as in the study of cosmic-ray tracks (Katz and Kobetich 1969). Alternatively, we can integrate the probability radially to yield the cross section for the interaction of a single ion with the target (Katz 1978b; Waligórski, Loh, and Katz 1987).

4.7 Hittedness

In radiobiology we are not yet able to measure the effect produced by the interaction of a single ion with a target. Yet this ability to measure is of central importance in estimating the effects of GCR in spaceflight. We can describe the interaction of a single ion with a target with the cross section. In track theory we wish to know whether a single particle, be it electron, proton, α-particle, or whatever, is capable of inducing the tested end point with observable probability. We characterize these interactions through the concept of *hittedness*, borrowed from biological target theory (Dertinger and Jung 1970). For a specific irradiation the appropriate hittedness is either the number of interactions between charged particles and target needed to induce the end point or the number of incident particles that must bombard the target, whichever is smaller. If either a single particle or a single interaction leads to the event, we will observe exponential response, as predicted by the

cumulative Poisson distribution. If two electrons are required for the event, we expect to observe a response described by the two-or-more-hit cumulative Poisson distribution. But the inactivation may take place through the transit of a single α-particle. In that case we expect to observe that the response to α-particles is one or more hit. We characterize the hittedness of a detector by its response to electrons or to gamma rays. Experimentally, if the response to the dose of gamma rays is exponential, we speak of a one-or-more-hit detector.

4.8 The One-Hit Detector

Most commonly, radiation detectors can be described as one-or-more-hit detectors. We imagine the detector to be a collection of targets—sometimes explicit, as in photographic emulsion, and sometimes implicit, as in a Fricke dosimeter or in alanine. Each of these targets is capable of responding to the transit of a single electron of appropriate energy. The response is exponential; that is, it is linear at low dose and sublinear at high dose as the available targets tend to have been inactivated. Saturation or overkill occurs at high dose. For one-hit detectors the response to heavy ions is also exponential with dose or fluence.

To calculate the inactivation cross section for a one-hit detector, we first find $P(D)$, the probability for target inactivation, as a function of the dose D of gamma rays. Next we fold this into the average radial dose distribution about an ion's path, to find the probability for target inactivation $P(t)$ at radial distance t. We integrate $P(t)$ radially to find the action cross section σ. When targets out to about three target diameters are all inactivated, we simply use the point distribution of dose in our calculations. If we must take into account effects closer than three target radii from the ion's path it is necessary to average the dose in the extended targets to accommodate the dose gradient. Averaging is necessary because the radial dose falls off essentially inversely as the square of the radial distance increases to a limit determined by the maximum delta-ray penetration. This limiting distance, determined essentially by the speed of the ion, places an upper limit on the action cross section that is observed experimentally with very heavy ions as thindown. (*Thindown* is named after the appearance of the tracks of heavy ions in electron-sensitive emulsions, where the stopping end of a track looks like a sharpened pencil.) Typically for these detectors the cross section increases with an increase in $(Z^*/\beta)^2$ to a maximum (typically unrelated to target size) and then declines in thindown.

The RBE is equal to $\sigma E_0/L$, where E_0 is the $1/e$ dose, or the dose for 37 percent survival. For one-hit detectors the RBE never exceeds one. The magnitude of the cross section is approximately determined by the radial distance at which the dose equals E_0. We may speak of the cross section as approximating the size of the damaged region, but it is inappropriate to speak of track size without specifying the end point. It is easy to estimate the cross section of a heavy ion with the grains of a nuclear emulsion from a microphotograph by estimating the radial distance at which about 63 percent of the grains are developed. At 63-percent development, we note that for insensitive emulsions where the track resembles a string of beads, the cross section is less than the grain size, whereas for a sensitive emulsion where the track resembles a hairy rope, the cross section may be orders of magnitude greater than the grain size.

Our first venture into the one-hit detector was made for dry enzymes and viruses (Butts and Katz 1967). This work was followed by a model for the response of nuclear emulsions (Katz and Kobetich 1969), of scintillation counters (Katz and Kobetich 1968), of thermoluminance detectors (TLD's), of alanine (Waligórski et al. 1989), and for *Escherichia coli B* (Katz and Zachariah 1991). There are indications that the plastic CR-39, used as an etchable track detector, is also a one-hit detector (Katz 1984).

The global applicability of the model of the one-hit detector to a wide variety of detectors whose mechanisms are vastly different from each other is at first thought to be rather astonishing. It arises simply from the fact that in each case the end point is stimulated by the passage of a single electron through the target volume.

4.9 Supralinearity and the Linear Quadratic Model

If a system has both one-hit and two-hit targets having different radiosensitivities and populations, we must expect that response will be linear at low dose, quadratic at intermediate doses, and saturating at high dose. We call the variable response *supralinear* and have proposed such a model to explain supralinearity in TLD-100 (Katz 1978a). Note that the concept of a two-hit target requires only that two incident electrons are needed to stimulate the end point. The response may arise after processing as well as in the initial interactions, for the present model treats each detector as a black box. But if there are not two varieties of response, we cannot understand supralinearity in this model. Nor can we understand how a detector whose response to gamma rays is exponential can exhibit an RBE with

heavy ions greater than one unless there are temporal effects hinging on the time difference between gamma-ray and delta-ray exposures. Such a time difference between hits appears explicitly in a kinetics model that may provide an approach to temporal effects.

In the same way, we do not understand the rationale for using the linear quadratic formula to fit radiobiological data if there are not two types of targets within a cell. We note that the formula is simply the first two terms of a series expansion and is usually applied to data of very limited dynamic range. Further we note that for radiations of different quality, there is no theory that can reliably predict the values of either the linear or the quadratic term. Nevertheless, these terms are liberally interpreted with such phrases as "could be" or "might be," though with equal validity one might insert "not."

Those who prefer to interpret data on the basis of hypothetical mechanisms whose details are rarely accessible via experiment may object to our parametric formulations. Yet the track-structure model and its experimental parameters should not be dismissed lightly, for they may suggest mechanistic interpretations that supersede those presently popular (Goodhead 1989). We note that Newton's laws were stimulated by Kepler's phenomenology and that quantum theory was stimulated by Planck's exercise in curve fitting.

4.10 Cell Survival Model

As detectors, biological cells require special consideration. For other detectors we assume, as in the case of nuclear emulsions, that the target has a characteristic size and no internal structure. The response of these detectors is then characterized by the parameters E_0, the dose of gamma rays at which there is an average of one hit per target, a_0, the sensitive site radius, and C, the hittedness. We also sometimes introduce a dimensionless track-structure parameter κ proportional to $E_0 a_0^2$. Biological cells, however, have internal targets. We imagine the cells to resemble a bean bag in which the cell nucleus is the bag and the targets are the beans. We take it that the beans are one-hit in character but that m of the beans must be inactivated to generate the observed response. We also imagine that the beans are well distributed throughout the bag so that an energetic ion passing through the bag has the possibility for inactivating m beans. Such a model makes it possible to understand why flatted cells respond differently to α-particles than rounded ones do.

In this model the observed cross section is related to the size of the bean bag and the variation of response with LET is related to the properties of the beans. To set up a model of cellular response, we calculate the cross section for a hypothetical cluster of m overlapping beans and then assume that the cross section for the bean bag is proportional to that of the cluster (Katz, Sharma, and Homayoonfar 1972). Because our model is based on the radial distribution of dose from delta rays, it automatically predicts thindown. For mammalian cells the fitted value of the κ parameter suggests that the bean radius is about 1 μm, and thus the target for cell killing may be a chromosome.

5. Mathematical Track-Structure Model of Cell Survival and Applications

Detailed descriptions of the track model of cell survival have been given elsewhere (see, for example, Katz, Sharma, and Homayoonfar 1972). Here we present only the main concepts of the model and list the equations used in our calculations. Following our earlier studies of the appearance of particle tracks in nuclear emulsion (Katz and Kobetich 1969), the model distinguishes between the grain-count regime, where inactivations occur randomly along the particle's path, and the track-width regime, where the inactivations are distributed like a hairy rope. The transition from the grain-count to track-width regime takes place at $Z^{*2}/\kappa\beta^2 \approx 4$; lower values are in the grain-count regime and higher values are in the track-width regime. The quality κ is a parameter of the track-structure model that combines both the target size and the characteristic dose of gamma rays at which there is an average of one hit per target. As in nuclear emulsions we speak of a thindown regime where the cross section is limited by the kinematic constraint on delta-ray energies, but has nothing to do with the Bragg peak in stopping power or with the changing effective charge of a slowing-down ion.

To accommodate for the capacity of cells to accumulate sublethal damage, two modes of inactivation are identified, namely ion kill (intratrack) and gamma kill (intertrack). In these two inactivation modes, the statistical character of the inactivation changes rather than the fundamental physical interaction. Effects are in terms of dose rather than the number of electrons passing through the nucleus. We do not find justification for considering the stopping end of an electron track as a source of ion kill nor do we consider the radial separation of a heavy-ion track into core producing ion kill and penumbra producing gamma kill.

The cell survival model uses Z^{*2}/β^2 as a plotting parameter superior to LET, now in wide use. At the stopping end of a track, at highest LET, even this

parameter fails because in the thindown regime the cross section depends on β, the relative speed of the ion. In the thindown regime the cross section is sometimes plotted against energy per unit mass, a related parameter. The model bases the meaning of low LET on the comparison of Z^{*2}/β^2 with κ. Similarly, *low* dose means low compared with E_0. The model explains why plots of extrapolated cross section from the tail of a survival curve tend to be single-valued functions of LET at low LET (response is dominated by gamma kill) and why they are multiple valued with Z at high LET (response is dominated by ion kill and thindown). It explains why plots of RBE versus LET for biological cells pass through a maximum when about half the intersected cells are killed in ion kill. It predicts that the RBE for lighter ions will be greater than the RBE for heavy ions at the same LET and the same survival level. This inequality is because of the structure of particle tracks. At the same LET, the heavier ions move faster. Its delta rays are fewer but more energetic and gamma kill is more likely, which reduces the RBE.

5.1 Gamma Kill

Cells not inactivated in the ion-kill mode can be sublethally damaged by delta rays from the passing particle and then inactivated in the gamma-kill mode by cumulative addition of sublethal damage from delta rays from other passing ions. Survival in the gamma-kill mode is taken to follow the m-target statistics of inactivation by secondary electrons from X-ray or gamma-ray photons.

5.2 Mathematical Formalism

In the grain-count regime the surviving fraction of a cellular population whose radiosensitivity parameters are m, E_0, σ_0, and κ, after track-segment irradiation with an ion dose D of a fluence of F particles of charge number Z, effective charge value Z^*, relative speed β, and stopping power L (LET_∞), is found from the expression

$$\frac{N}{N_0} = \Pi_i \times \Pi_\gamma \tag{1}$$

where ion-kill fraction is

$$\Pi_i = \exp(-\sigma F) \tag{2}$$

and where gamma-kill fraction is

$$\Pi_\gamma = 1 - \left[1 - \exp\left(\frac{-D_\gamma}{E_0}\right)\right]^m \tag{3}$$

The gamma-kill dose is

$$D_\gamma = (1 - P)D \tag{4}$$

where the ion-kill probability is

$$P = \frac{\sigma}{\sigma_0} = \left[1 - \exp\left(\frac{-Z^{*2}}{\kappa\beta^2}\right)\right]^m \tag{5}$$

In the track-width regime, where $P > 0.98$, we take

$$\Pi_\gamma = 1 \tag{6}$$

and find σ from the track width, which increases linearly with Z^*/β as the inactivation cross section increases with Z^{*2}/β^2 up to the limit set by the maximum radial range of delta rays. This is the thindown region.

To find the cross section in the track-width regime, including the thindown region, a separate calculation must be made. First the target cross section S for targets of radius a_0 is found from

$$S = 2\pi \int_0^\infty t\, dt (1 - e^{-\overline{D}(t,a_0)/E_0})^m \tag{7}$$

where $\overline{D}(t, a_0)$ is the average radial dose in the target of radius a_0. The target radius a_0 is found from κ and E_0 according to

$$\kappa = (E_0 a_0^2) \times (5 \times 10^6 \mathrm{erg\text{-}cm}) \tag{8}$$

with multitarget response to gamma rays characterized by E_0 and m found for the cell. The S value must be multiplied by the ratio of the plateau value of the action cross section σ_0 to the plateau value of the target cross section S_0 to yield the cellular action cross section in the track-width regime (Katz et al. 1971). In this region we assume there is no gamma-kill dose, though in the outer reaches of the track width some small fraction of the energy lost by the ion is deposited in the gamma-kill mode.

To calculate RBE at a given kill (transformation) or survival level we use the definition

$$\mathrm{RBE} = \frac{D_x}{D} \tag{9}$$

where

$$D_x = -E_0 \left\{\ln\left[1 - \left(1 - \frac{N}{N_0}\right)^{1/m}\right]\right\} \tag{10}$$

is the equivalent X-ray dose, and D is the corresponding ion dose.

All calculations pertain to water, so the ion dose is always

$$D = FL \tag{11}$$

Where cross sections and RBE's are calculated from the final slope of the survival curves, we refer to the cross section and RBE as extrapolated, and in the grain-count regime we write

$$\sigma_{\text{ext}} = \sigma_0 P + \frac{(1-P)L}{E_0} \tag{12}$$

and

$$\text{RBE}_{\text{ext}} = (\sigma_0 E_0 / L)P + (1-P) \tag{13}$$

To calculate the effective charge value of an ion of charge number Z moving with a relative velocity β, we use the expression (Barkas 1963)

$$Z^* = Z[1 - \exp(-125\beta Z^{-2/3})] \tag{14}$$

We calculate the stopping power and range in water of an ion of atomic number Z with the expression

$$L(Z,E) = L(p,E) \left(\frac{Z^*}{Z_p^*}\right)^2 \tag{15}$$

where Z^* and Z_p^* are the effective charges of the ion and proton, respectively, and $L(p,E)$ is the stopping power, in water, of a proton at the same energy per nucleon E.

At low fluence, where ions are sufficiently far apart that intertrack effects are unlikely, we can neglect the contribution from gamma kill. Under this circumstance RBE is

$$\text{RBE} = E_0 \left(\frac{\sigma}{L}\right)^{1/m} D^{(1/m-1)} \tag{16}$$

This value is applicable to low doses of neutrons as well as to the effects of GCR's (Katz and Cucinotta 1991) and agrees with the measurements of Bettega et al. (1990) down to doses of 0.01 Gy.

In order to determine the RBE for mixed radiation fields, our model requires knowledge of the particle-energy spectrum of the radiation field. We then find the totality of effects due to ion kill, add to that sum the gamma-kill doses including the dose from gamma rays, find from this value the ion-kill and the gamma-kill survival probability, and take their product to be the surviving fraction of irradiated cells. We have done these calculations for neutrons admixed with gamma rays (Katz, Sharma, and Homayoonfar 1972), for range-modulated heavy-ion beams (Roth and Katz 1980), and most recently for cosmic rays (Cucinotta et al. 1990).

5.3 Cell Killing, Chromosome Aberrations, and Transformations

Our treatment of transformations (Waligórski, Sinclair, and Katz 1987) is based on data obtained with the BEVALAC accelerator by Yang et al. (1985). We use the same form of equations for cell killing and take cell killing and transformation to be independent processes that take place along the same particle track. Our parameters for Chinese hamster cells are based on the data of Skarsgard et al. (1967) whereas the parameters for *Tradescantia* are based on the data of Underbrink et al. (1978). We have extracted parameters from data obtained with X rays and neutron irradiations of two different energy spectra, ignoring possible gamma-ray contamination. The parameters for T-1 cells of human origin are taken from Todd (1967). The separate sets of parameters for cell survival, chromosome aberration, and transformation are shown in table 1 (Katz and Huang 1991). Two sets of parameters are shown when the data do not permit a clear distinction between them.

5.4 Target Fragmentation Effects

High-energy protons passing through tissue will occasionally cause nuclear reactions that produce low-energy, high-LET ions from the tissue itself. The target fragments, in turn, will be a source of delta rays that should contribute to biological damage locally in the tissue matrix. The differential fluence F_j (Wilson 1977) describes the local source of target fragments:

$$F_j = \frac{1}{L(Z_j,E)} \int_E^\infty \frac{d\Sigma_j(E')}{dE'} F_p(E_p)\, dE' \tag{17}$$

where j is the fragment label, L is the stopping power, Σ_j is the macroscopic nuclear production cross section, and F_p is the fluence of protons with energy E_p. An effective action cross section for the proton dressed by the local target fragments (nuclear stars) is now written as

$$\sigma^* = \sigma_p(E_p) + \frac{1}{F_p(E_p)} \sum_j \int_0^\infty F_j(E_j)\, \sigma_j(E_j)\, dE_j \tag{18}$$

where σ_p and σ_j are given by the Katz formalism (eq. (5)). The gamma-kill dose for the proton and

target fragments is written as

$$D_\gamma = D_{\gamma,p}(E_p) + \sum_j \int_0^\infty F_j(E_j)\ L(Z_j, E_j)\ \left[1 - P_j(E_j)\right]\ dE_j \tag{19}$$

The production energy spectra for the target fragments are expressed as (Wilson et al. 1989)

$$\frac{d\Sigma_j}{dE} = \frac{\Sigma_j(E_p)\ \sqrt{E}}{\left(2\pi E_{0j}^3\right)^{1/2}}\ e^{-E/2E_{0j}} \tag{20}$$

where the average energy of the fragment is given by $3E_{0j}$.

The fragmentation parameters that are described in this paper are discussed in Wilson, Townsend, and Khan (1989). The light-ion production cross sections are from Bertini's Monte Carlo results (Anon. 1968) and the Silberberg-Tsao empirical model is used for the heavier fragments (Silberberg, Tsao, and Shapiro 1976). The average energy of the tissue fragments is related to the momentum width that is measured experimentally (Greiner et al. 1975), which Wilson, Townsend, and Khan (1989) fit empirically. The largest uncertainties exist for light-ion production ($A = 7$ and 9) and for energies below 100 MeV. Elastic recoils and meson production above several hundred MeV will also contribute to the action cross section and should be added. Stopping power in tissue is from the work of Wilson (1983), which is based on the Ziegler (1980) analysis.

The solid line in figure 1 displays the fragment LET component derived from equation (17) for 1-GeV protons in water. The dotted and dashed lines show the contributions from the secondary proton fragments and α-particles, respectively.

The proton action cross section for cell survival of V79 Chinese hamster cells versus the proton energy is shown in figure 2. The cellular response parameters are given in table 1. These parameters are compared with the data of Hall et al. (1978) for survival of Chinese hamster cells where the characteristic X-ray dose E_0 is taken as 2.9 Gy, as found from their X-ray data and with the remaining parameters the same as given by table 1. The dotted line in figure 2 shows the contributions from primary ionizations; the dashed line shows contributions from secondary ions; and the solid line shows total ion contributions. The oxygen and nitrogen fragments contribute partially to the cross section in the track-width regime. The decreasing proton LET with increasing energy leads to complete domination by target fragments above about 50 MeV. The shape of the action cross section in figure 2 directly reflects the nuclear absorption cross section in tissue. We expect a further increase above several hundred MeV when meson production is included in the cross section. In table 2, the individual contributions to the action cross section for V79 Chinese hamster cells are shown for several proton energies. Secondary protons and α-particles are dominant, with broad spectra of tissue fragments making nonnegligible contributions. Primary proton contributions make up an insignificant fraction of the action cross section above 100 MeV, and the relatively slow change with energy of the nuclear production cross sections leads to a plateau in the action cross section at high proton energies.

Figure 3 shows the action cross section versus proton LET with the calculations of figure 2 corresponding to high-LET protons depicted to 0.1 MeV. The behavior of the cross section below 0.5 keV/μm shows the dominance of the tissue secondaries (nuclear stars). At about 0.2 keV/μm, the proton LET reaches a minimum and then increases, which is the origin of the "hook" in figure 3 at the lowest LET values. It would be interesting to test our results for the proton cross section by experiment. Results herein assume an equilibrium in the local secondary fluence spectra and are sensitive to interface effects (Cucinotta, Hajnal, and Wilson 1990) and the composition of the host media of the cell culture.

Figure 4 shows the proton gamma-kill dose divided by E_0 versus proton energy. The primary ionization is the dotted line and the solid line includes the effects of fragments. Secondary ion production has a negligible effect on intertrack effects, except at the highest energies, where a small contribution is seen.

Cellular parameters obtained for survival and neoplastic transformations of C3H10T½ cells obtained from the experiments of Yang et al. (1985) are given in table 1. The large uncertainties in the transformation data of Yang et al. in table 1 should lead to similar uncertainties in the transformation parameters. Parameter sets were found from data for instantaneous and delayed plating of the cells after irradiation. In this paper only the delayed plating case is considered. Using the parameter sets, general agreement with the measured RBE values was found (Waligórski, Sinclair, and Katz 1987). The single-particle-inactivation cross section with the target fragmentation of equation (18) neglected is shown in figures 5 and 6 for cell death and cell transformation, respectively, as a function of the energy of the passing ion. The target fragmentation contribution (the second term in eq. (18)) for protons has been evaluated as shown in figures 7 and 8. For protons

the effects of the target fragments, shown as a dashed line, dominate over the proton direct ionization (dotted line) at high energy. For high-LET particles (low energy), direct ionization dominates and target fragmentation effects become negligible. A simple scaling by $A_j^{1/2}$ relates the proton target fragment term to ions of mass A_j. The resulting effective action cross sections for cell death and cell transformation are plotted in figures 9 and 10, respectively. We note that the low-energy ^{56}Fe component of the GCR spectra extends into the track-width regime where $\sigma > \sigma_0$ and is not represented in the present calculations. The resultant error introduced into the present calculation is small.

5.5 Survival Curves and Proton RBE

Cell survival curves for 10-, 100-, and 1000-MeV protons are shown as a function of absorbed dose in figures 11(a)–(c). The dotted lines shown in the figures indicate the primary ionization contributions and the solid lines indicate the added effects of the target fragment contributions. Results show the importance of secondary ion production for increasing energy. For example, at 1000 MeV the increase in cell death due to the fragments does not lead to substantial changes in RBE at high doses, as shown in figure 11(c). It is in the initial portion of the survival curves where the ion-kill mode causes large differences in RBE when compared with gamma rays.

Proton RBE for survival of Chinese hamster cells versus absorbed dose is shown in figure 12, and all curves include the effects of target fragmentation. We note that in figure 12, proton fluence is $F_p = 6.24D/\text{LET}$, with F_p in protons/μm^2. The rise in RBE at low dose or fluence, where single proton tracks dominate, is directly attributed to ion kill from both primary protons at 10 MeV and nuclear fragments at the higher energies. Not shown are RBE calculations neglecting the target fragments, which are nearly identical to the results for the 10-MeV proton in figure 12 and are almost identical to unity for the 100- and 1000-MeV protons. The low-dose behavior of the RBE can be seen from equation (16), where a dependence on $D^{-2/3}$ is found for $m = 3$ (from the data of Skarsgard et al. (1967) in table 1). This effect is supported experimentally as discussed below (Cucinotta et al. 1991c).

5.6 RBE of 160-MeV Plateau Region Protons

Cell survival experiments have been performed at the Harvard Cyclotron for the purpose of determining the RBE of the protons. The V79 Chinese hamster cells cultured in vitro were irradiated in the plateau region of the Bragg curve and in a spread-out Bragg peak by Hall et al. (1978). Using the track model and the high-energy nucleon transport code BRYNTRN of Wilson et al. (1988 and 1989), we compare the survival measurements and RBE determinations for attached cells in the plateau region of the 160-MeV-proton Bragg curve.

The nucleon transport code BRYNTRN solves the coupled proton-neutron transport problem for high energies in the straight-ahead approximation with multiple-scattering and straggling effects ignored. Target fragments with $A > 1$ are transported by taking the production collision density, which is given as F_j in equation (17). The respective Boltzmann equations for proton and neutron transport are

$$\left[\frac{\partial}{\partial x} - \frac{\partial}{\partial E}L(Z_p, E) + \Sigma_p(E)\right]\Phi_p(x, E) = \sum_j \int_E^\infty f_{pj}(E, E')\ \Phi_j(x, E')\ dE' \quad (21)$$

and

$$\left[\frac{\partial}{\partial x} + \Sigma_n(E)\right]\Phi_n(x, E) = \sum_j \int_E^\infty f_{nj}(E, E')\ \Phi_j(x, E')\ dE' \quad (22)$$

where Φ_j is the particle flux of type j particles at position x with energy E; $L(Z_j, E)$ is the proton stopping power; $\Sigma_p(E)$ and $\Sigma_n(E)$ are proton and neutron total cross sections, respectively; and $f_{ij}(E, E')$ represents the differential cross sections for elastic and inelastic processes. As described by Wilson and Lamkin (1975), the Boltzmann equations (21) and (22) are solved with a characteristic transformation to reduce the problem to a set of coupled integral equations with boundary conditions at $x = 0$, which are then solved numerically. More details on the method of solution and the nuclear scattering data base are given by Wilson et al. (1988 and 1989). The Bragg curve obtained from BRYNTRN for 160-MeV protons in water is shown in figure 13 with measurements of Verhey et al. (1979). In figure 13 the squares represent the primary dose and the circles the total dose including secondary production. Calculations are normalized to the peak of the experimental Bragg curve. Straggling and multiple-scattering effects, which are not included here, both contribute significantly at the peak of the Bragg curve. We

consider the plateau region to be where the high-energy assumptions are approximately true.

At energies of 160 MeV, nuclear recoils from elastic scattering provide a sizable correction to the secondary ion production represented by target fragmentation. Elastic nuclear scattering is represented by the Born term of the optical model renormalized to the total scattering cross section in the BRYNTRN code. This representation of elastic nuclear scattering is fairly accurate for integral quantities above 100 MeV, but it breaks down at lower energies because of multiple scattering, nuclear medium corrections, and especially Coulomb effects. The correction to the proton action cross section from elastic scattering is shown in table 3 for several energies and is included in the following comparisons.

Results for the surviving fraction of suspended V79 Chinese hamster cells irradiated by ^{60}Co gamma rays and plateau region of a 160-MeV proton beam (Hall et al. 1978) are shown in figure 14. The dashed line is the fit to the experimental gamma-ray survival curve, the dotted line (barely distinguishable from the gamma-ray response) is the contribution from primary protons only, and the solid line depicts calculations that include the effects of nuclear reactions. The characteristic gamma-ray dose E_0 is taken as 2.9 Gy to reproduce the experimental gamma-ray curve with the other response parameters given above. The dashed and dotted lines are nearly identical, an indication that high-energy protons minus the effects of nuclear force indeed act as gamma rays. Agreement with the data is fair and indicates that the modeling of nuclear fragmentation made in this paper is somewhat lacking. Figure 15 presents our results for the proton RBE and the values obtained with the analysis methods of Kellerer and Brenot (1973) as discussed by Hall et al. (1978). The "bare" proton RBE has a value of 1 (not shown), except at the lowest doses, where a small contribution from ion kill gives a slight increase. The calculations of the proton RBE presented in figure 15 show good agreement with the experimentally obtained values, with the increasing RBE at low doses shifted to lower values than experiment. A second analysis methodology that assumes only that the dose-effect curve is convex but is otherwise shape independent was used to derive RBE values (Hall et al. 1978) and they are shown in figure 16 with present predictions. The rise in RBE values at low dose as predicted in equation (16) is clearly seen in the calculations and the experimental values. Also shown in figure 16 are our calculations neglecting nuclear reactions, the values being almost exactly 1 for all doses.

5.7 Cell Survival in HZE Beams

The HZE transport problem has been solved and related to the Bragg curve (Wilson 1977 and 1983) for monoenergetic unidirectional ion beams. The Bragg curves we calculate also provide the values for fluence estimates for the exposure conditions of biological samples yet to be analyzed. Errors in the Bragg curve translate directly into errors in exposure levels for comparisons with experimental response data.

Calculations of the relative ionization ratio for ^{40}Ar at 514 MeV/nucleon are compared with the experiments of Blakely et al. (1979) in figure 17. The effects of nuclear secondaries are seen to be most important near and beyond the Bragg peak. Survival for aerobic and hypoxic T-1 cells of human origin has been calculated with the Katz parameters in table 1 for several locations along the beam line within a water column for three different ion beams of C, Ne, and Ar. Calculations include both projectile as well as target fragments. Results for the ^{12}C beam experiments (Blakely et al. 1979) are shown in figure 18. Effects of overlapping delta rays are clearly apparent except near the Bragg peak, where the sigmoid appearance has all but disappeared. The sigmoid shape returns downstream from the Bragg peak, where the overlapping delta-rays from adjacent ions again contribute to the exposure. Note that the oxygen effect has all but vanished near the Bragg peak whereas hypoxic cells show considerable radiation resistance both upstream and downstream from the Bragg peak. Results of our calculations for ^{20}Ne beams are shown in figure 19. Results for the ^{20}Ne beam are qualitatively similar to those for ^{12}C beams. The region over which the sigmoid appearance is suppressed is greatly expanded in the Bragg peak region. Oxygen enhancement is greatly diminished 1 cm before and after the Bragg peak, as can be seen in figure 20. This fact is of potential importance to radiation therapy. The sigmoid behavior is virtually nonexistent for the ^{40}Ar beam exposures, as shown in figure 20. Obviously, at some great distance downstream, the sigmoid shape will appear because only light fragments will survive. No experiments were conducted in this region.

5.8 Cell Damage for the GCR Spectrum

To apply the cellular track model to the mixed-radiation fields found in space, we need to make the appropriate replacement of the cross section and particle fluence number σF with the particle field quantities and their corresponding cross sections. The ion-kill term, which will now contain a projectile source term (including projectile fragments) and a

target fragment term, is written as

$$\sigma F = \sum_j \int dE_j\ \Phi_j(x, E_j)\ \sigma_j(E_j)$$

$$+ \sum_\alpha \sum_j \int dE_\alpha\ dE_j\ \Phi_\alpha(x, E_\alpha : E_j)\ \sigma_\alpha(E_\alpha) \quad (23)$$

where the second term is the contribution of nuclear fragments produced locally in the biological medium (Cucinotta et al. 1991a). This contribution may also be written in terms of an effective action cross section σ^* for the passing ion, whose track is dressed by the local target fragments (nuclear stars), as

$$\sigma F = \sum_j \int dE_j\ \Phi_j(x, E_j)\ \sigma^*(E_j) \quad (24)$$

The gamma-kill dose fraction becomes

$$D_\gamma = \sum_j \int dE_j\ \Phi_j(x, E_j)\ [1 - P_j(E_j)]\ S_j(E_j)$$

$$+ \sum_j \sum_\alpha \int dE_j\ dE_\alpha\ \Phi_\alpha(x, E_\alpha : E_j)$$

$$\times\ [1 - P_\alpha(E_\alpha)]\ S_\alpha(E_\alpha) \quad (25)$$

Equations (23) and (25) are used in equations (2) and (3), respectively. The summations over all particle types in equations (23) and (25) represent the addition of probabilities from all ions in the radiation field that contribute to the end point under study.

The cellular track model was applied to predict the fraction of C3H10T½ cells killed or transformed for 1 yr in deep space at solar minimum behind typical spacecraft shielding. The GCR environment was taken from the Naval Research Laboratory code (Adams, Silberberg, and Tsao 1981). Aluminum shielding was considered with a local region of tissue for the cell cultures. Tables 4 and 5 contain individual particle fluences and absorbed doses, respectively, for the protons, α-particles, $Z = 3$ to 9 ions (labeled L-Z), and $Z = 10$ to 28 ions (labeled H-Z) as determined by the Langley GCR code (Wilson, Townsend, and Badavi 1987). Results for the fraction of C3H10T½ cells killed and transformed for 1 yr at solar minimum behind aluminum shielding are listed in tables 6 and 7, respectively. The gamma-kill mode was of negligible importance in the calculations, and this unimportance indicates that biological damage in deep space from GCR particles at the cellular level will indeed result from the action of single particles. The importance of the target terms in biological effects for low-LET protons and α-particles is quite apparent. The results also indicate that the HZE component of the GCR spectrum is the most damaging for small shielding depths. At large depths the HZE components break up and cause proton buildup with increasing shield depth. At large depths the protons dominate the biological effects. In comparing individual charge components, we see that the H-Z particles have a reduced effectiveness for the transformation end point.

Also listed in tables 6 and 7 are the values of RBE for the two end points. In table 8 we show the present RBE values beside the average QF values taken from Townsend et al. (1990), who used the same transport code. The fact that RBE and QF values are nearly equal at small depths is somewhat coincidental. We note that the QF is independent of the fluence level; this independence is not true for the Katz model. The Katz model indicates a substantial increase in risk, at higher shielding levels, compared with QF's given in report no. 26 of the International Committee on Radiological Protection (Anon. 1977).

The RBE values show a simple scaling with exposure time for the GCR particles, as can be seen from equations (9), (10), and (2) when ion kill dominates. Here we find for

$$\frac{N}{N_0} \approx 1 \quad (26)$$

with

$$\sigma F \ll 1 \quad (27)$$

that

$$\mathrm{RBE} = \frac{E_0}{L}\ \sigma^{1/m}\ F^{[-1+(1/m)]} \quad (28)$$

Then, scaling RBE as a function of duration in deep space to the 1-yr value τ_1 for a duration period of τ (with $F = n\tau$) gives (Cucinotta et al. 1991a and 1991b)

$$\mathrm{RBE}(\tau) = \left(\frac{\tau}{\tau_1}\right)^{[-1+(1/m)]} \mathrm{RBE}(\tau_1) \quad (29)$$

As a result, a one-hit ($m = 1$) system RBE becomes fluence independent, as expressed by

$$\mathrm{RBE}(\tau) = \mathrm{RBE}(\tau_1) \quad (30)$$

a two-hit ($m = 2$) system is expressed by

$$\mathrm{RBE}(\tau) = \frac{\mathrm{RBE}(\tau_1)}{(\tau/\tau_1)^{1/2}} \quad (31)$$

and a three-hit ($m = 3$) system is expressed by

$$\mathrm{RBE}(\tau) = \frac{\mathrm{RBE}(\tau_1)}{(\tau/\tau_1)^{2/3}} \tag{32}$$

Results of this scaling approximation agree quite well with calculations from the Katz model, as shown in table 9, where values obtained with the approximations of equation (28) are shown in parentheses as scaled from the 1-yr RBE values taken from table 8, and results of the calculations are shown without parentheses. The extremely large RBE values that would be obtained for small values of τ are due to the choice of energetic photons as the reference radiation.

6. Concluding Remarks

Over the past 25 years Katz and coworkers have developed a model of particle tracks that began with nuclear emulsions and subsequently has been extended to other detectors and to the biological effects of high linear energy transfer (LET) radiations. This model requires as input information knowledge of the particle-energy spectrum of the radiation environment as well as the dose of gamma rays. Calculations of the effects of beams of protons, of heavy ions, and of energetic neutrons have been hindered because of the lack of a model of such beams that included both projectile and target fragmentation. A beam model created at NASA Langley Research Center remedied this neglect. Through it we have been able to validate both the track theory of biological effects and the beam model by comparison of our calculated radiobiological end points with ground-based measurements for proton and heavy-ion beams. Based on this validation we have initiated calculations of biological effects in space vehicles in selected orbits, incorporating knowledge of the distribution of solar and galactic cosmic rays to be encountered there. We know of no other way to estimate the biological damage in space flight at the very low fluences of heavy ions to be encountered there.

NASA Langley Research Center
Hampton, VA 23681-0001
August 20, 1992

7. References

Anon. 1968: *MECC-7 Intranuclear Cascade Code, 500-MeV Protons on O-16. I4C Analysis Codes* (Programmed for H. W. Bertini). Available from Radiation Shielding Information Center, Oak Ridge National Lab.

Anon. 1977: *Recommendations of the International Commission on Radiological Protection.* ICRP Publ. 26, Pergamon Press.

Adams, J. H., Jr.; Silberberg, R.; and Tsao, C. H. 1981: *Cosmic Ray Effects on Microelectronics. Part I The Near-Earth Particle Environment.* NRL Memo. Rep. 4506-Pt. I, U.S. Navy. (Available from DTIC as AD A103 897.)

Barkas, Walter H. 1963: *Nuclear Research Emulsions I. Techniques and Theory.* Academic Press, Inc.

Bettega, D.; Calzolari, P.; Ottolenghi, A.; and Talloni Lombardi, L. 1990: Oncogenic Transformation Induced by High and Low LET Radiations. *Radiat. Prot. Dosim.*, vol. 31, nos. 1–4, pp. 279–283.

Blakely, Eleanor A.; Tobias, Cornelius A.; Yang, Tracy C. H.; Smith, Karen C.; and Lyman, John T. 1979: Inactivation of Human Kidney Cells by High-Energy Monoenergetic Heavy-Ion Beams. *Radiat. Res.*, vol. 80, no. 1, pp. 122–160.

Butts, J. J.; and Katz, Robert 1967: Theory of RBE for Heavy Ion Bombardment of Dry Enzymes and Viruses. *Radiat. Res.*, vol. 30, no. 4, pp. 855–871.

Cucinotta, Francis A.; Hajnal, Ferenc; and Wilson, John W. 1990: Energy Deposition at the Bone-Tissue Interface From Nuclear Fragments Produced by High-Energy Nucleons. *Health Phys.*, vol. 59, no. 6, pp. 819–825.

Cucinotta, Francis A.; Katz, Robert; Wilson, John W.; Townsend, Lawrence W.; Nealy, John E.; and Shinn, Judy L. 1991a: *Cellular Track Model of Biological Damage to Mammalian Cell Cultures From Galactic Cosmic Rays.* NASA TP-3055.

Cucinotta, Francis A.; Atwell, William; Weyland, Mark; Hardy, Alva C.; Wilson, John W.; Townsend, Lawrence W.; Shinn, Judy L.; and Katz, Robert 1991b: *Radiation Risk Predictions for Space Station* Freedom *Orbits.* NASA TP-3098.

Cucinotta, Francis A.; Katz, Robert; Wilson, John W.; Townsend, Lawrence W.; Shinn, Judy; and Hajnal, Ferenc 1991c: Biological Effectiveness of High-Energy Protons: Target Fragmentation. *Radiat. Res.*, vol. 127, pp. 130–137.

Curtis, S. B.; Townsend, L. W.; Wilson, J. W.; Powers-Risius, P.; Alpen, E. L.; and Fry, R. J. M. 1992: Fluence-Related Risk Coefficients Using the Harderian Gland Data as an Example. *Adv. Space Res.*, vol. 12, no. 2–3, pp. (2)407–(2)416.

Dertinger, Hermann; and Jung, Horst 1970: *Molecular Radiation Biology.* Springer-Verlag.

Goodhead, D. T. 1988: Spatial and Temporal Distribution of Energy. *Health Phys.*, vol. 55, no. 2, pp. 231–240.

Goodhead, Dudley T. 1989: Relationships of Radiation Track Structure to Biological Effect: A Re-Interpretation of the Parameters of the Katz Model. *Nucl. Tracks Radiat. Meas.*, vol. 16, no. 2/3, pp. 177–184.

Greiner, D. E.; Lindstrom, P. J.; Heckman, H. H.; Cork, Bruce; and Bieser, F. S. 1975: Momentum Distributions of Isotopes Produced by Fragmentation of Relativistic ^{12}C and ^{16}O Projectiles. *Phys. Review Lett.*, vol. 35, no. 3, pp. 152–155.

Hall, Eric J.; Kellerer, Albrecht M.; Rossi, Harald H.; and Lam, Yuk-Ming P. 1978: The Relative Biological Effectiveness of 160 MeV Protons. II: Biological Data and Their Interpretation in Terms of Microdosimetry. *Int. J. Radiat. Oncol. Biol. Phys.*, vol. 4, no. 11 & 12, pp. 1009–1013.

Katz, Robert; and Kobetich, E. J. 1968: Response of NaI(Tl) to Energetic Heavy Ions. *Phys. Review*, vol. 170, second ser., no. 2, pp. 397–400.

Katz, Robert; and Kobetich, E. J. 1969: Particle Tracks in Emulsion. *Phys. Review*, vol. 186, second ser., no. 2, pp. 344–351.

Katz, R.; Ackerson, B.; Homayoonfar, M.; and Sharma, S. C. 1971: Inactivation of Cells by Heavy Ion Bombardment. *Radiat. Res.*, vol. 47, pp. 402–425.

Katz, Robert; Sharma, S. C.; and Homayoonfar, M. 1972: The Structure of Particle Tracks. *Topics in Radiation Dosimetry, Supplement 1*, F. H. Attix, ed., Academic Press, Inc., pp. 317–383.

Katz, Robert 1978a: High LET Constraints of Low LET Survival. *Phys. Med. Biol.*, vol. 23, no. 5, pp. 909–916.

Katz, Robert 1978b: Track Structure Theory in Radiobiology and in Radiation Detection. *Nucl. Track Detect.*, vol. 2, no. 1, pp. 1–28.

Katz, Robert 1984: Formation of Etchable Tracks in Plastics. *Nucl. Tracks & Radiat. Meas.*, vol. 8, nos. 1–4, pp. 1–8.

Katz, R.; Dunn, D. E.; and Sinclair, G. L. 1985: Thindown in Radiobiology. *Radiat. Prot. Dosim.*, vol. 13, nos. 1–4, pp. 281–284.

Katz, R.; Sinclair, G. L.; and Waligórski, M. P. R. 1986: The Fricke Dosimeter as a 1-Hit Detector. *Nucl. Tracks Radiat. Meas.*, vol. 11, no. 6, pp. 301–307.

Katz, Robert; and Huang, Guo-Rong 1989: Track "Core" Effects in Heavy Ion Radiolysis. *Int. J. Radiat. Appl. Instrum., Part C: Radiat. Phys. Chem.*, vol. 33, no. 4, pp. 345–349.

Katz, Robert 1990: Cross Section. *Int. J. Radiat. Appl. Instrum., Part A: Appl. Radiat. Isot.*, vol. 41, no. 6, pp. 563–567.

Katz, Robert; Loh, Kim Sum; Daling, Luo; and Huang, Guo-Rong 1990: An Analytic Representation of the Radial Distribution of Dose From Energetic Heavy Ions in Water, Si, LiF, NaI, and SiO_2. *Radiat. Effects & Defects in Solids*, vol. 114, pp. 15–20.

Katz, Robert 1991: On the Normalized Yield (Events/Rad/Dalton) of Biological Molecules Irradiated With Energetic Heavy Ions. *Int. J. Radiat. Appl. Instrum., Part C: Radiat. Phys. Chem.*, vol. 37, no. 2, pp. 373–374.

Katz, Robert; and Cucinotta, F. A. 1991: RBE vs. Dose for Low Doses of High-LET Radiations. *Health Phys.*, vol. 60, no. 5, pp. 717–718.

Katz, R.; and Huang, G. 1991: Radiosensitivity Parameters for Cell Survival in *Tradescantia* and for Chromosome Aberrations in Chinese Hamster Cells. *Radiat. Prot. Dosim.*, vol. 31, pp. 372–374.

Katz, Robert; and Varma, Matesh N. 1991: Radial Distribution of Dose. *Physical and Chemical Mechanisms in Molecular Radiation Biology*, W. A. Glass and M. N. Varma, eds., Plenum Press, pp. 163–180.

Katz, R.; and Zachariah, R. 1991: *E Coli B* Modeled as a 1-Hit Detector. *Radiation Research: A Twentieth-Century Perspective — Volume I: Congress Abstracts*, J. D. Chapman, W. C. Dewey, and G. F. Whitmore, eds., Academic Press, Inc., p. 117.

Kellerer, Albrecht M.; and Brenot, Jean 1973: Nonparametric Determination of Modifying Factors in Radiation Action. *Radiat. Res.*, vol. 56, no. 1, pp. 28–39.

Roth, Rose Ann; and Katz, Robert 1980: Heavy Ion Beam Model for Radiobiology. *Radiat. Res.*, vol. 83, pp. 499–510.

Silberberg, R.; Tsao, C. H.; and Shapiro, M. M. 1976: Semiempirical Cross Sections, and Applications to Nuclear Interactions of Cosmic Rays. *Spallation Nuclear Reactions and Their Applications*, B. S. P. Shen and M. Merker, eds., D. Reidel Publ. Co., pp. 49–81.

Skarsgard, L. D.; Kihlman, B. A.; Parker, L.; Pujara, C. M.; and Richardson, S. 1967: Survival, Chromosome Abnormalities, and Recovery in Heavy-Ion- and X-Irradiated Mammalian Cells. *Radiat. Res.*, suppl. 7, pp. 208–221.

Todd, Paul 1967: Heavy-Ion Irradiation of Cultured Human Cells. *Radiat. Res.*, suppl. 7, pp. 196–207.

Townsend, Lawrence W.; Nealy, John E.; Wilson, John W.; and Simonsen, Lisa C. 1990: *Estimates of Galactic Cosmic Ray Shielding Requirements During Solar Minimum.* NASA TM-4167.

Underbrink, A. G.; Huczkowski, J.; Woch, B.; Gedlek, E.; Cebulska-Wasilewska, A.; Litwiniszyn, M.; and Kasper, E. 1978: *The Relationship of Different Somatic Mutations Induced by Neutrons and X Rays to Loss of Reproductive Integrity in Tradescantia Stamen Hairs.* Rep. No. 1039/B, Inst. of Nuclear Physics (Kraków, Poland).

Verhey, L. J.; Koehler, A. M.; McDonald, J. C.; Goitein, M.; Ma, I-C.; Schneider, R. J.; and Wagner, M. 1979: The Determination of Absorbed Dose in a Proton Beam for Purposes of Charged-Particle Radiation Therapy. *Radiat. Res.*, vol. 79, pp. 34–54.

Waligórski, M. P. R.; Hamm, R. N.; and Katz, R. 1986: The Radial Distribution of Dose Around the Path of a Heavy Ion in Liquid Water. *Nucl. Tracks & Radiat. Meas.*, vol. 11, no. 6, pp. 309–319.

Waligórski, M. P. R.; Loh, Kim Sun; and Katz, R. 1987: Inactivation of Dry Enzymes and Viruses by Energetic Heavy Ions. *Radiat. Phys. & Chem.*, vol. 30, no. 3, pp. 201–208.

Waligórski, M. P. R.; Sinclair, G. L.; and Katz, R. 1987: Radiosensitivity Parameters for Neoplastic Transformations in C3H10T½ Cells. *Radiat. Res.*, vol. 111, pp. 424–437.

Waligórski, M. P. R.; Danialy, G.; Loh, Kim Sun; and Katz, R. 1989: The Response of the Alanine Detector After Charged-Particle and Neutron Irradiations. *Int. J. Radiat. Appl. Instrum., Part A: Appl. Radiat. Isot.*, vol. 40, no. 10–12, pp. 923–933.

Wilson, John W.; and Lamkin, Stanley L. 1975: Perturbation Theory for Charged-Particle Transport in One Dimension. *Nucl. Sci. & Eng.*, vol. 57, no. 4, pp. 292–299.

Wilson, John W. 1977: *Analysis of the Theory of High-Energy Ion Transport.* NASA TN D-8381.

Wilson, John W. 1983: *Heavy Ion Transport in the Straight Ahead Approximation.* NASA TP-2178.

Wilson, John W.; Townsend, Lawrence W.; and Badavi, Forooz F. 1987: Galactic HZE Propagation Through the Earth's Atmosphere. *Radiat. Res.*, vol. 109, no. 2, pp. 173–183.

Wilson, John W.; Townsend, Lawrence W.; Chun, Sang Y.; Buck, Warren W.; Khan, Ferdous; and Cucinotta, Frank, 1988: BRYNTRN: *A Baryon Transport Computer Code—Computation Procedures and Data Base.* NASA TM-4037.

Wilson, John W.; Townsend, Lawrence W.; and Khan, Ferdous 1989: Evaluation of Highly Ionizing Components in High-Energy Nucleon Radiation Fields. *Health Phys.*, vol. 57, no. 5, pp. 717–724.

Wilson, John W.; Townsend, Lawrence W.; Nealy, John E.; Chun, Sang Y.; Hong, B. S.; Buck, Warren W.; Lamkin, S. L.; Ganapol, Barry D.; Khan, Ferdous; and Cucinotta, Francis A. 1989: BRYNTRN: *A Baryon Transport Model.* NASA TP-2887.

Yang, Tracy Chui-Hsu; Craise, Laurie M.; Mei, Man-Tong; and Tobias, Cornelius A. 1985: Neoplastic Cell Transformation by Heavy Charged Particles. *Radiat. Res.*, vol. 104, pp. S-177–S-187.

Ziegler, J. F. 1980: *Handbook of Stopping Cross-Sections for Energetic Ions in All Elements.* Volume 5 of *The Stopping and Ranges of Ions in Matter*, J. F. Ziegler, ed., Pergamon Press, Inc.

Table 1. Parameters for Cell Survival, Aberrations, and Transformations

Biological end point	m	κ	E_0, Gy	σ_0, cm^2
$CH2B_2$ Chinese hamster cells (Skarsgard et al. 1967):				
Survival	3	1100	1.82	4.3×10^{-7}
Abnormal metaphases	3	900	1.82	3.0×10^{-7}
Chromatid exchanges	2	1400	25	6.5×10^{-9}
C3H10T½ mouse cells (Yang et al. 1985):				
Survival	3	750	1.7	5.0×10^{-7}
Transformations	2	750	180	1.2×10^{-10}
Transformations	3	475	50	7.0×10^{-11}
Tradescantia (Underbrink et al. 1978):				
Survival	2	1000	2.1	3.5×10^{-7}
Survival	1.5	1900	2.6	4.0×10^{-7}
Human T-1 cells (Todd 1967):				
Survival (aerobic)	2.5	1000	1.7	6.7×10^{-7}
Survival (hypoxic)	2.5	1300 (1450)[a]	4.6 (5.2)[a]	6.7×10^{-7}

[a]Two sets of parameters are shown because the data do not permit a clear distinction between them.

Table 2. Target Fragment Contributions to Proton Action Cross Section for V79 Chinese Hamster Cells

Z_j	A_j	Target fragment contributions to proton cross section, σ, cm^2, for E_p of—		
		10 MeV	100 MeV	1000 MeV
1	1	4.58×10^{-12}	6.70×10^{-12}	7.14×10^{-12}
1	2	.21	.40	1.49
1	3	.10	.19	.22
2	3	.16	.34	.66
2	4	1.68	3.59	12.22
3	5	.32	.42	.65
3	6	.46	.53	.68
3	7	.04	.17	.42
4	6	.01	.07	.20
4	7	.36	.42	.49
4	8	.41	.51	.53
4	9	<.01	.04	.09
5	8	<.01	.04	.11
5	9	.10	.30	.32
5	10	.22	.35	.28
5	11	.02	.21	.35
6	10	<.01	.03	.08
6	11	.04	.41	.32
6	12	.50	1.00	.63
6	13	.14	.32	.24
6	14	<.01	.02	.03
7	12	<.01	.01	.04
7	13	.03	.09	.07
7	14	1.11	.82	.37
7	15	.02	.24	.41
8	14	<.01	.02	.05
8	15	.02	.56	.28
Primary proton contributions		32.61	0.05	<0.01
Total contributions		43.16	17.84	28.35

Table 3. Secondary Ion Production Contribution to Proton Action Cross Section for V79 Chinese Hamster Cells

E_p, MeV	Contribution to proton action cross section, σ, cm^2, for—	
	Elastic recoils	Fragmentation
100	1.13×10^{-11}	1.081×10^{-11}
150	.82	1.02
1000	.58	2.09

Table 4. Fluence for 1 Year at Solar Minimum Behind Aluminum Shielding

x, g/cm^2	Fluence, particles/cm^2, from—			
	Protons	α-particles	[a]L-Z	[b]H-Z
0	1.29×10^8	1.24×10^7	1.09×10^7	3.0×10^7
1	1.31	1.21	1.05	2.8
2	1.33	1.18	1.01	2.7
3	1.34	1.15	.98	2.5
5	1.36	1.10	.91	2.2
10	1.40	.97	.77	1.7
20	1.43	.77	.57	1.1

[a] Z = 3 to 9 ions.
[b] Z = 10 to 28 ions.

Table 5. Absorbed Dose for 1 Year at Solar Minimum Behind Aluminum Shielding

x, g/cm^2	Dose, cGy/yr, from—				
	Protons	α-particles	[a]L-Z	[b]H-Z	Total
0	6.2	3.0	2.8	5.0	17.1
1	6.3	2.7	2.5	3.6	15.1
2	6.8	2.6	2.4	3.3	15.1
3	7.1	2.6	2.3	3.1	15.0
5	7.6	2.4	2.1	2.7	14.8
10	8.5	2.1	1.7	2.0	14.3
20	9.5	1.7	1.1	1.1	13.4

[a] Z = 3 to 9 ions.
[b] Z = 10 to 28 ions.

Table 6. Fraction of C3H10T½ Cells Killed in Deep Space for 1 Year at Solar Minimum Behind Aluminum Shielding

x, g/cm^2	Fraction of cells killed by—				Total	RBE
	Protons	α-particles	[a]L-Z	[b]H-Z		
Including target fragments						
0	1.35×10^{-2}	0.46×10^{-2}	0.57×10^{-2}	2.08×10^{-2}	4.46×10^{-2}	7.1
1	.76	.15	.43	1.84	3.18	7.0
2	.80	.14	.41	1.69	3.04	6.9
3	.83	.14	.38	1.55	2.90	6.8
5	.88	.14	.34	1.32	2.68	6.7
10	.95	.12	.25	.91	2.22	6.5
20	1.02	.09	.15	.49	1.74	6.2
Without target fragments						
0	0.84×10^{-2}	0.37×10^{-2}	0.55×10^{-2}	2.08×10^{-2}	3.79×10^{-2}	6.7
1	.24	.06	.41	1.83	2.54	6.5
2	.28	.06	.39	1.68	2.41	6.3
3	.31	.06	.37	1.55	2.27	6.2
5	.35	.06	.33	1.31	2.04	6.1
10	.42	.05	.24	.91	1.61	5.7
20	.49	.04	.14	.48	1.15	5.3

[a] Z = 3 to 9 ions.
[b] Z = 10 to 28 ions.

Table 7. Fraction of C3H10T½ Cells Transformed in Deep Space for 1 Year at Solar Minimum Behind Aluminum Shielding

x, g/cm^2	Fraction of cells transformed—				Total	RBE
	Protons	α-particles	[a]L-Z	[b]H-Z		
Including target fragments						
0	5.2×10^{-6}	2.0×10^{-6}	3.1×10^{-6}	7.5×10^{-6}	1.78×10^{-5}	6.4
1	3.5	1.0	2.7	6.7	1.39	6.4
2	3.7	1.0	2.6	6.2	1.35	6.3
3	3.9	.9	2.4	5.7	1.29	6.3
5	4.2	.9	2.2	4.9	1.22	6.2
10	4.7	.8	1.7	3.5	1.06	6.0
20	5.2	.6	1.1	2.0	.88	5.7
Without target fragments						
0	3.2×10^{-6}	1.6×10^{-6}	3.1×10^{-6}	7.5×10^{-6}	1.53×10^{-5}	6.0
1	1.4	.6	2.7	6.7	1.13	5.8
2	1.6	.6	2.5	6.2	1.09	5.7
3	1.8	.6	2.4	5.7	1.05	5.6
5	2.1	.5	2.1	4.9	.97	5.4
10	2.5	.5	1.6	3.5	.82	5.2
20	3.0	.4	1.0	2.0	.64	4.9

[a] Z = 3 to 9 ions.
[b] Z = 10 to 28 ions.

Table 8. Comparison of Average Quality Factors[a] Versus RBE for Cell Death and Transformation

[One year in deep space at solar minimum]

x, g/cm^2	QF (b)	RBE for cell death	RBE for cell transformation
0	7.1	7.1	6.4
1	5.6	7.0	6.4
2	5.3	6.9	6.3
3	5.1	6.8	6.3
5	4.7	6.7	6.2
10	3.9	6.5	6.0
20	3.2	6.2	5.7

[a]Townsend et al. (1990).
[b]ICRP 26 (Anon. 1977).

Table 9. RBE for Cell Death and Transformation of C3H10T½ Cell for GCR Spectrum at Solar Minimum Behind Aluminum Shielding

[Values in parentheses scaled from 1-year value using eq. (29)]

x, g/cm^2	RBE values for time periods of		
	1 mo	1 yr	2 yr
Cell death			
0	33.2 (37.0)	7.1	4.8 (4.6)
1	33.2 (36.1)	7.0	4.7 (4.5)
3	32.4 (35.1)	6.8	4.5 (4.3)
Cell transformation			
0	22.3 (22.2)	6.4	4.6 (4.5)
1	22.0 (22.2)	6.4	4.5 (4.5)
3	21.6 (21.8)	6.3	4.4 (4.4)

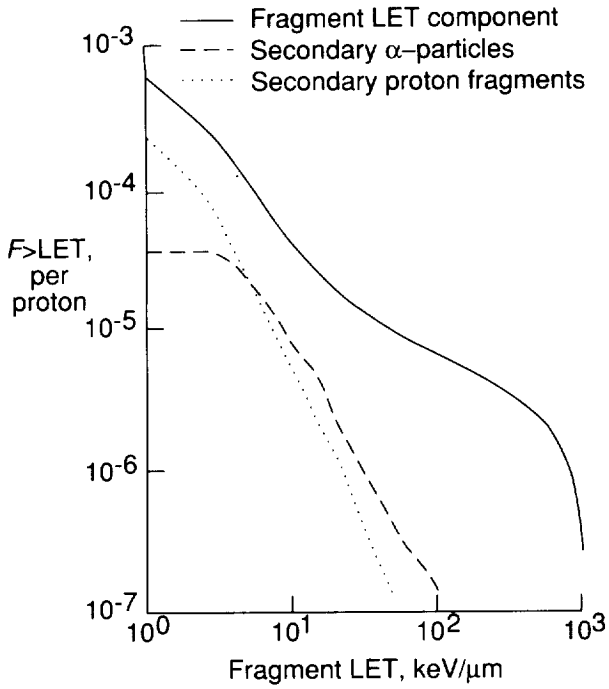

Figure 1. Integral LET spectra derived from equation (17) for nuclear fragments produced by 1-GeV protons in water.

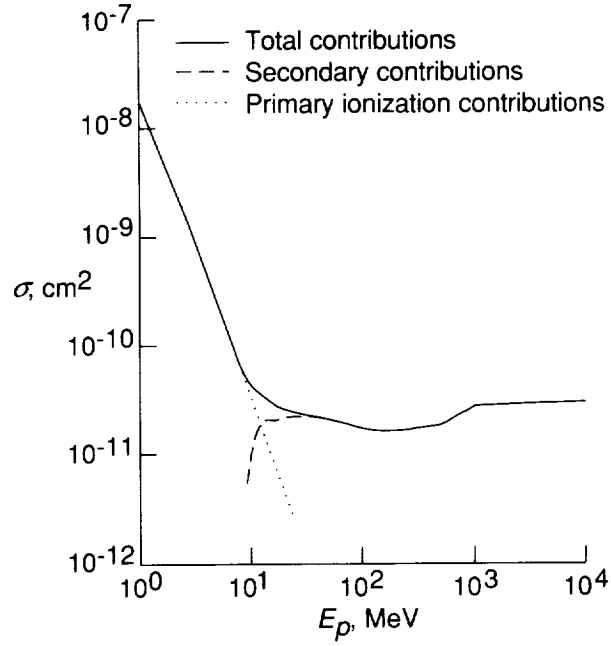

Figure 2. Calculated values of the proton action cross section for survival of V79 Chinese hamster cells versus proton energy.

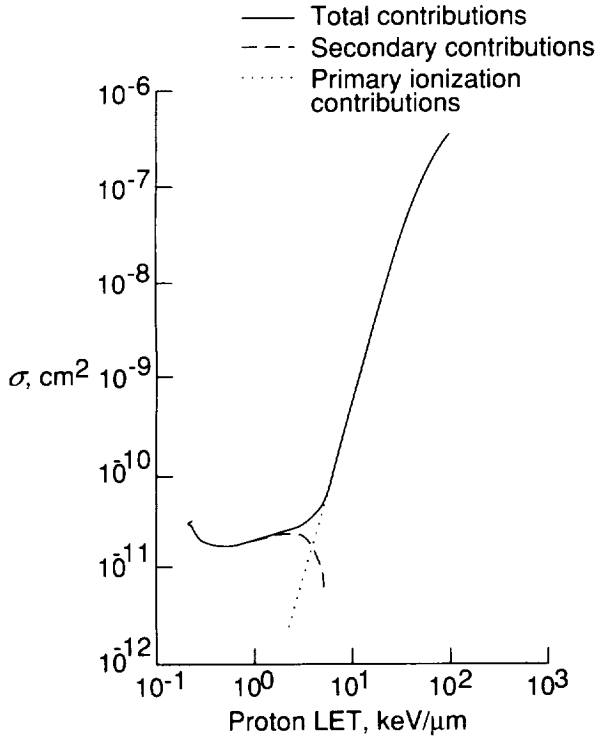

Figure 3. Calculated values of the proton action cross section for survival of V79 Chinese hamster cells versus proton LET.

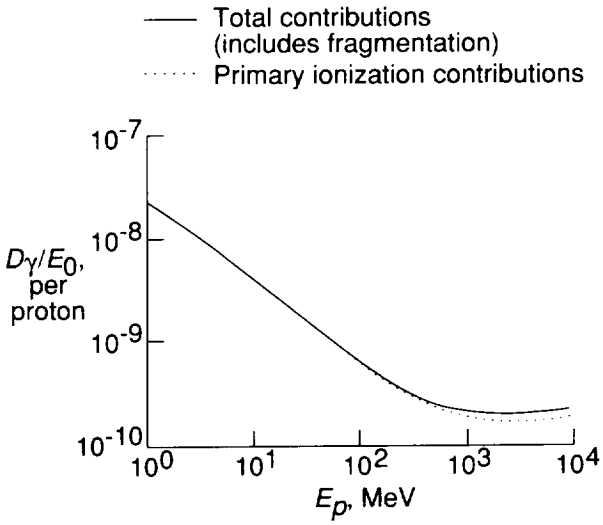

Figure 4. Calculated values of the proton gamma-kill dose for survival of V79 Chinese hamster cells versus proton energy.

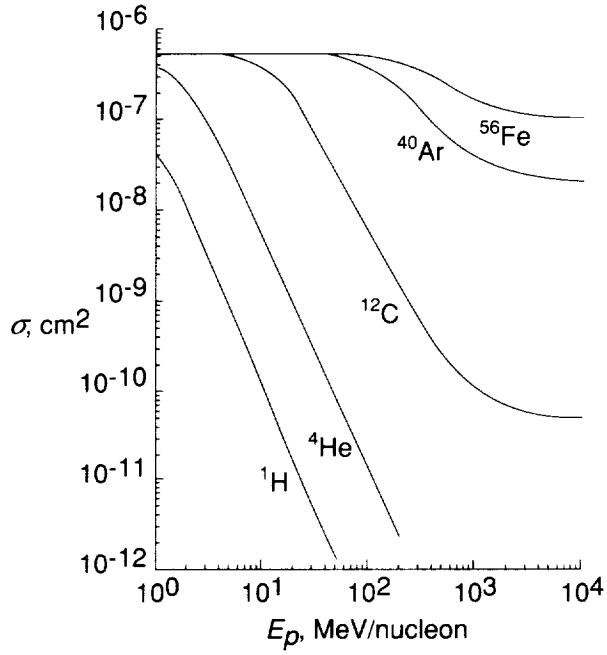

Figure 5. Cell-death action cross section for various ions in C3H10T½ cells according to Katz model for direct ionization effects only.

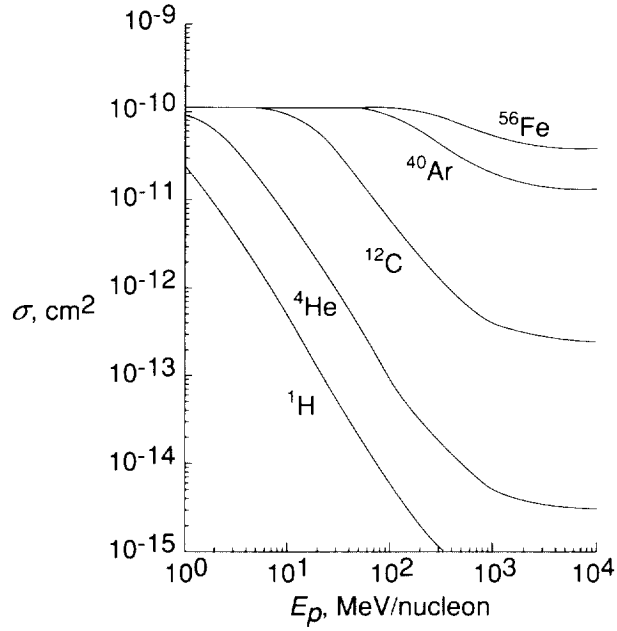

Figure 6. Cell-transformation action cross section for various ions in C3H10T½ cells according to Katz model.

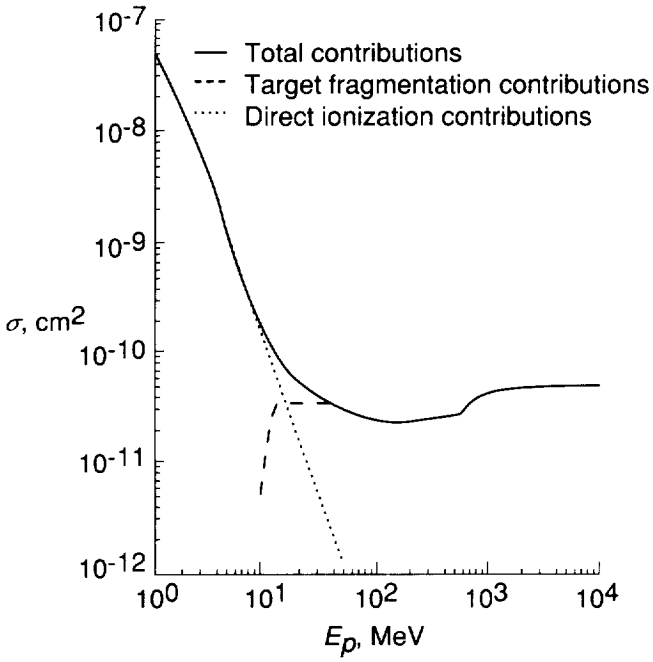

Figure 7. Cell-death action cross section including effects of nuclear reactions for protons in C3H10T½ cells according to Katz model.

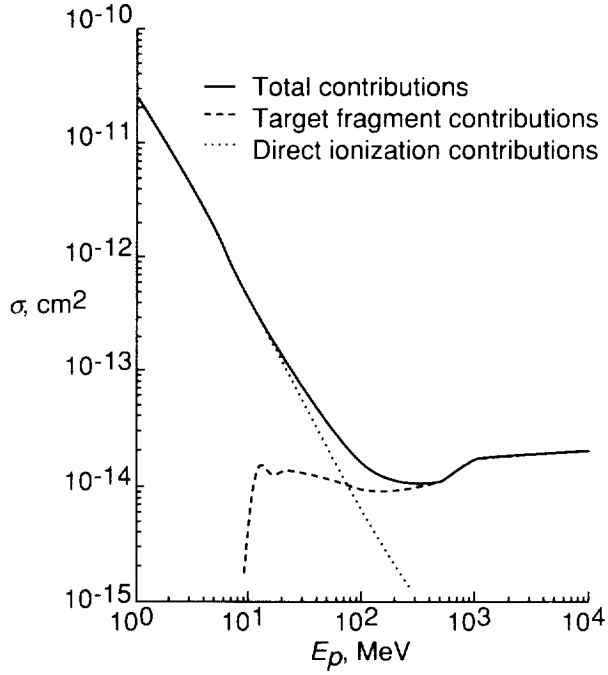

Figure 8. Cell-transformation action cross section including effects of nuclear reactions for protons in C3H10T½ cells according to Katz model.

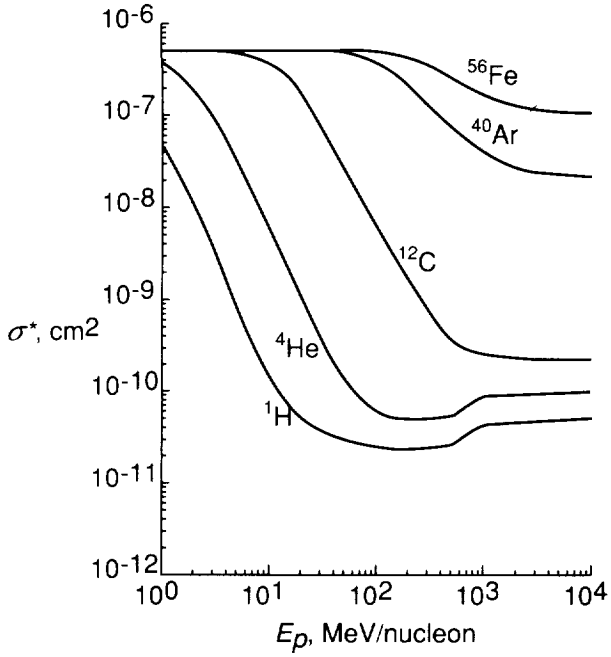

Figure 9. Cell-death effective action cross section including effects of nuclear reactions for various ions in C3H10T½ cells.

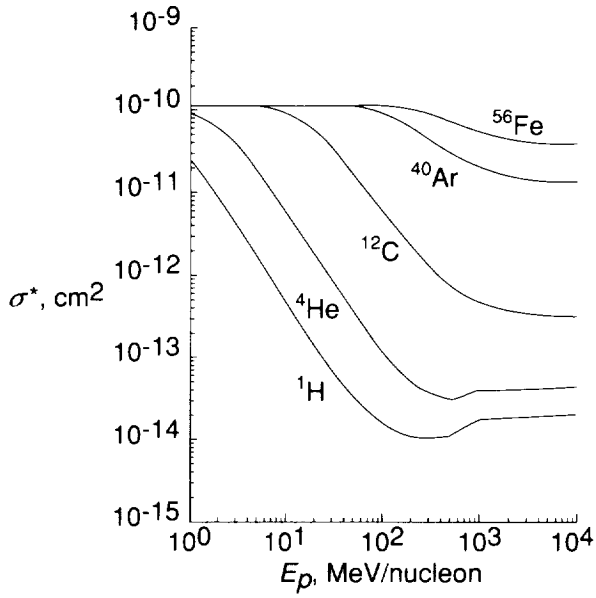

Figure 10. Cell-transformation effective action cross section including effects of nuclear reactions for various ions in C3H10T½ cells.

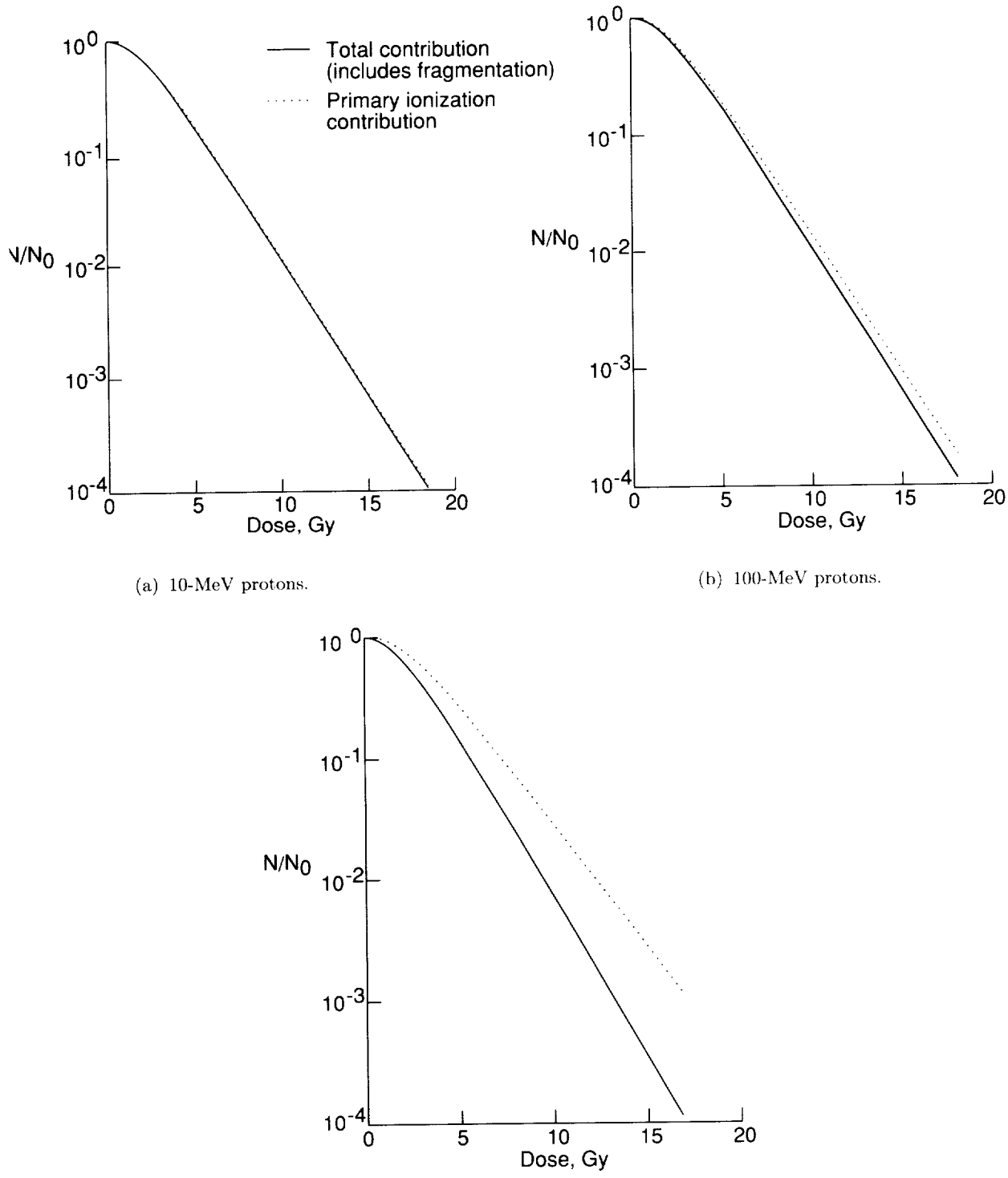

(a) 10-MeV protons.

(b) 100-MeV protons.

(c) 1000-MeV protons.

Figure 11. Calculated cell surviving fraction of Chinese hamster cells.

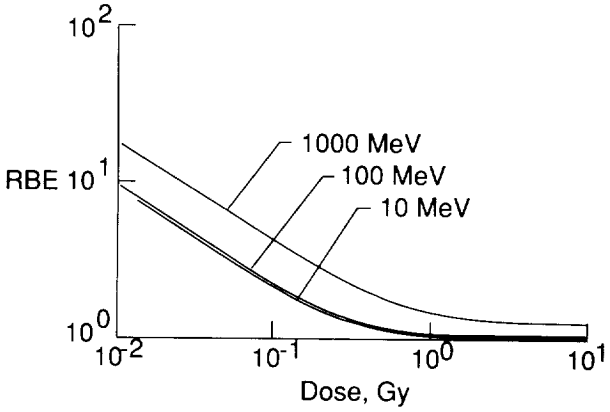

Figure 12. Calculations of proton RBE for survival of Chinese hamster cells versus absorbed dose.

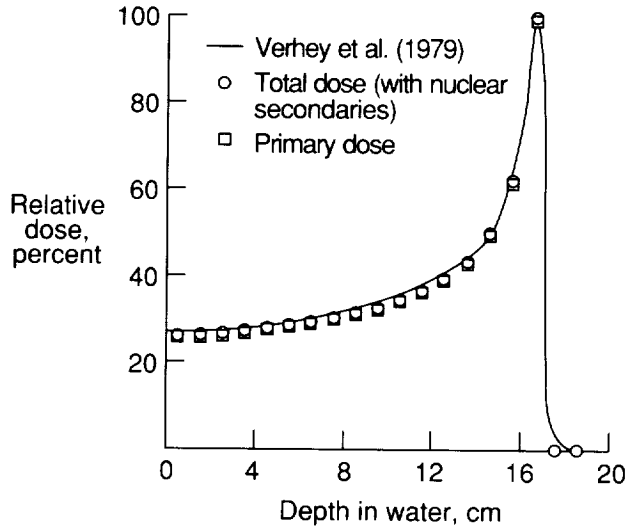

Figure 13. Depth-dose curve for unmodulated 160-MeV-proton beam in water.

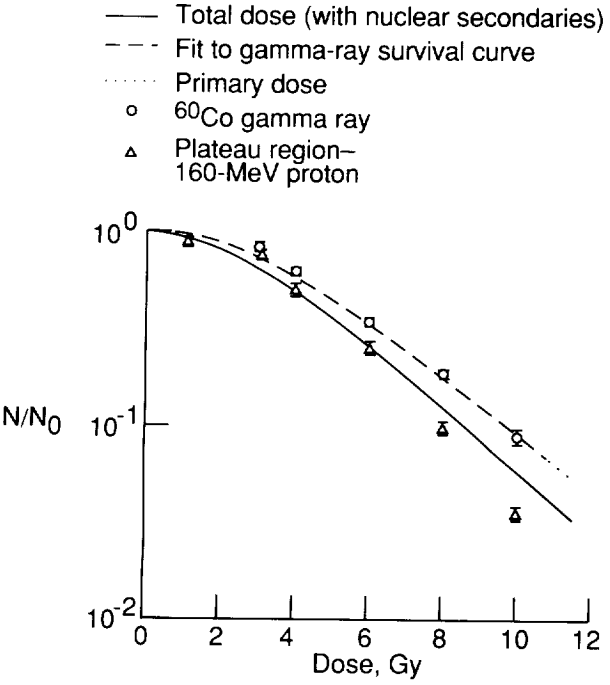

Figure 14. Survival for V79 Chinese hamster cells irradiated by ^{60}Co gamma rays and plateau-region 160-MeV protons (from Hall et al. 1978) are compared with calculations.

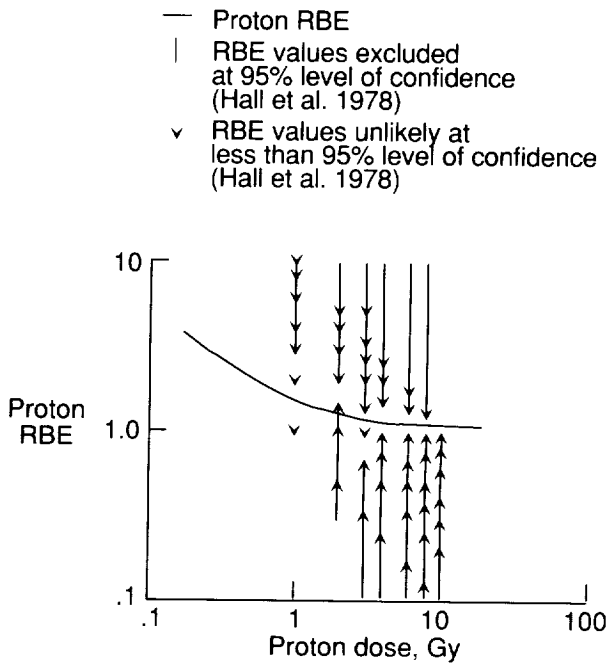

Figure 15. Proton RBE versus proton dose for V79 Chinese hamster cell survival in plateau region of 160-MeV-proton Bragg curve from first method described in Hall et al. (1978). Most likely RBE values fall in space between vertical bars.

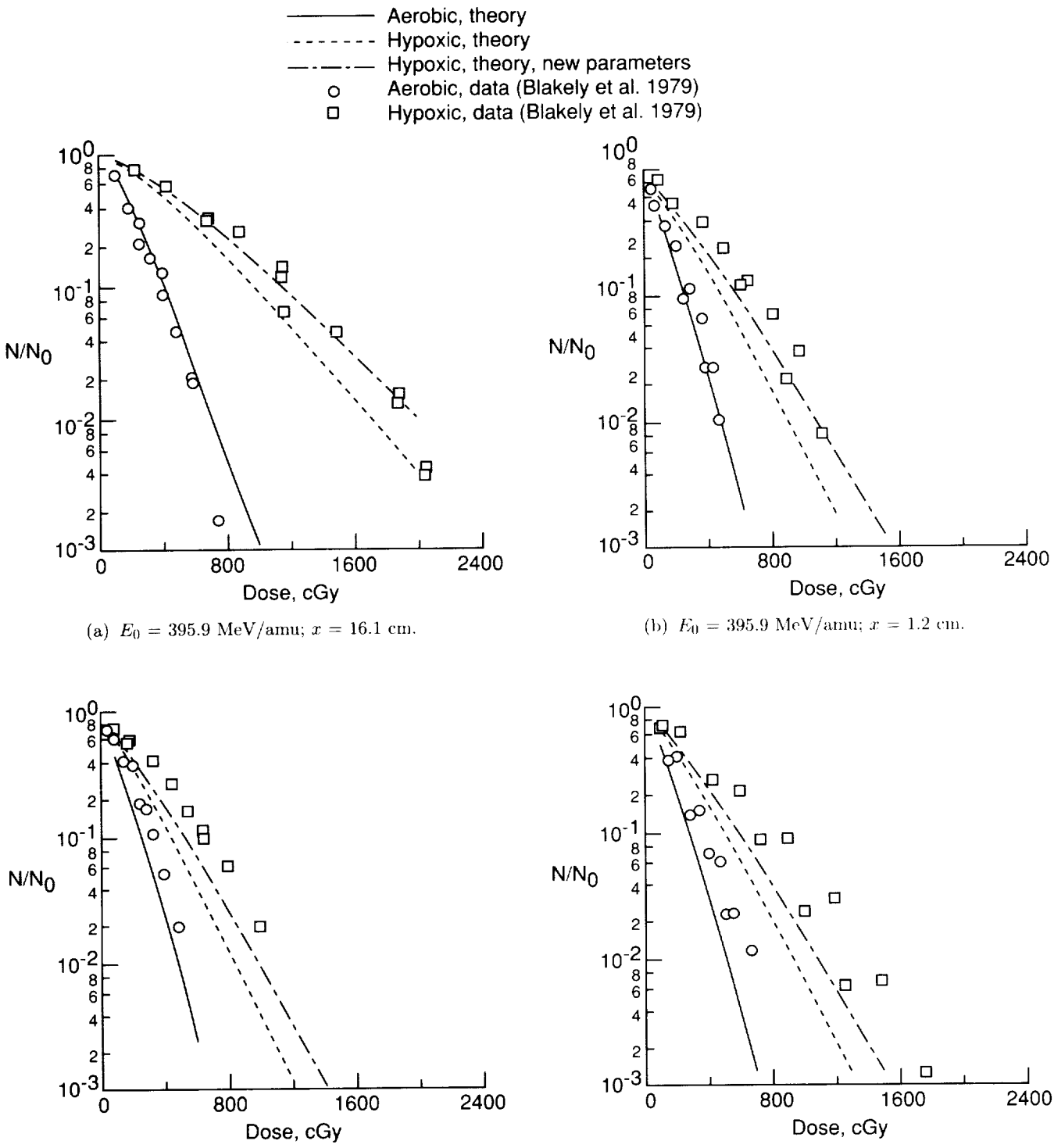

(a) $E_0 = 395.9$ MeV/amu; $x = 16.1$ cm.

(b) $E_0 = 395.9$ MeV/amu; $x = 1.2$ cm.

(c) $E_0 = 395.9$ MeV/amu; $x = -0.2$ cm.

(d) $E_0 = 395.9$ MeV/amu; $x = -2.0$ cm.

Figure 19. Cell survival as function of dosage at several locations relative to Bragg peak in ^{20}Ne beam.

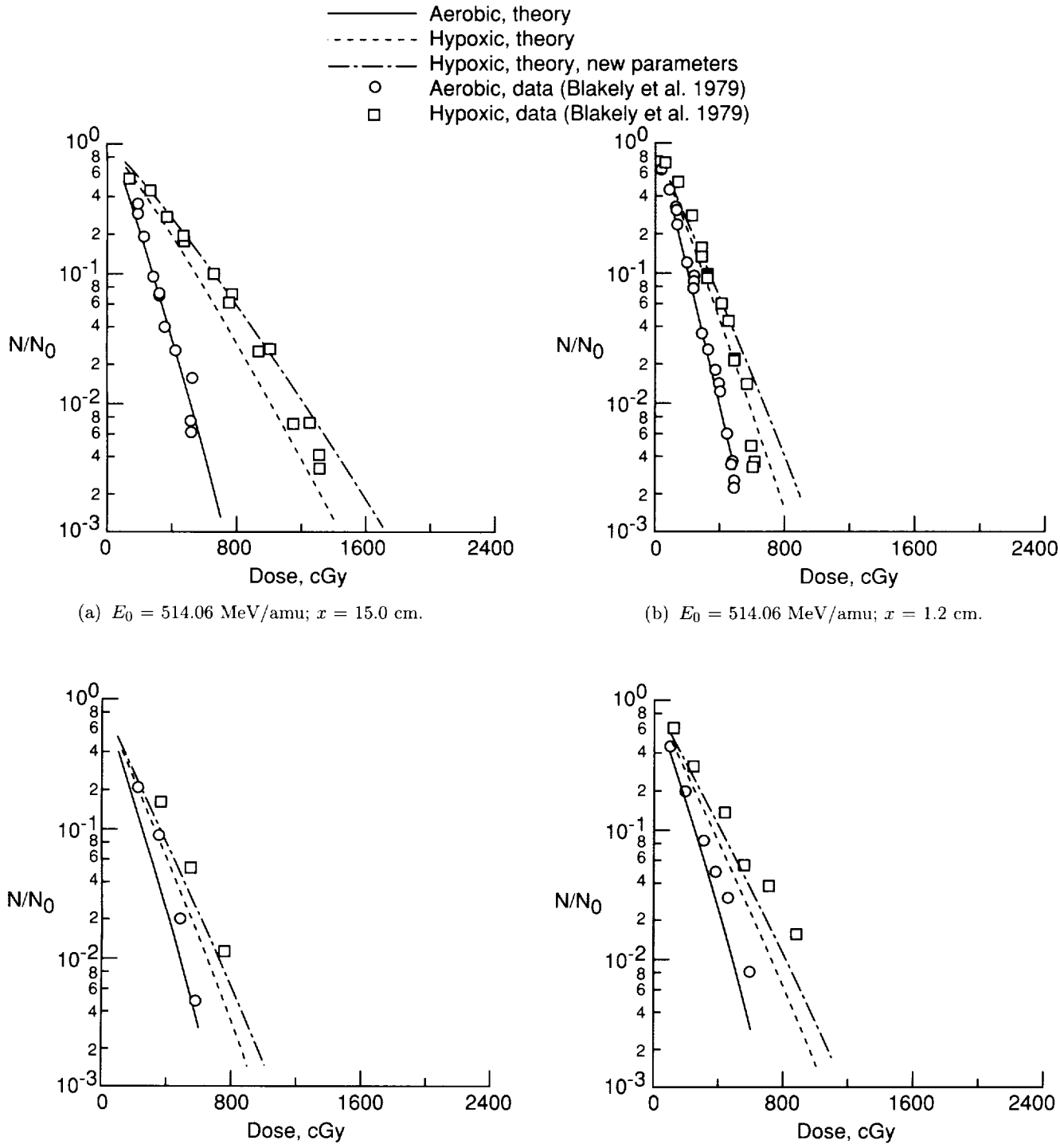

(a) $E_0 = 514.06$ MeV/amu; $x = 15.0$ cm.

(b) $E_0 = 514.06$ MeV/amu; $x = 1.2$ cm.

(c) $E_0 = 514.06$ MeV/amu; $x = -0.2$ cm.

(d) $E_0 = 514.06$ MeV/amu; $x = -2.0$ cm.

Figure 20. Cell survival as function of dosage at several locations relative to Bragg peak in ^{40}Ar beam.

REPORT DOCUMENTATION PAGE

Form Approved
OMB No. 0704-0188

1. AGENCY USE ONLY *(Leave blank)*	2. REPORT DATE	3. REPORT TYPE AND DATES COVERED
	October 1992	Technical Paper

4. TITLE AND SUBTITLE
Track Structure Model of Cell Damage in Space Flight

5. FUNDING NUMBERS
WU 199-04-16-11

6. AUTHOR(S)
Robert Katz, Francis A. Cucinotta, John W. Wilson, Judy L. Shinn, and Duc M. Ngo

7. PERFORMING ORGANIZATION NAME(S) AND ADDRESS(ES)
NASA Langley Research Center
Hampton, VA 23681-0001

8. PERFORMING ORGANIZATION REPORT NUMBER
L-17058

9. SPONSORING/MONITORING AGENCY NAME(S) AND ADDRESS(ES)
National Aeronautics and Space Administration
Washington, DC 20546-0001

10. SPONSORING/MONITORING AGENCY REPORT NUMBER
NASA TP-3235

11. SUPPLEMENTARY NOTES
Katz: University of Nebraska, Lincoln, NE; Cucinotta, Wilson, and Shinn: Langley Research Center, Hampton, VA; Ngo: Old Dominion University, Norfolk, VA.

12a. DISTRIBUTION/AVAILABILITY STATEMENT
Unclassified–Unlimited

Subject Category 52

12b. DISTRIBUTION CODE

13. ABSTRACT *(Maximum 200 words)*
The phenomenological track-structure model of cell damage is discussed. A description of the application of the track-structure model with the NASA Langley transport code for laboratory and space radiation is given. Comparisons to experimental results for cell survival during exposure to monoenergetic, heavy-ion beams are made. The model is also applied to predict cell damage rates and relative biological effectiveness for deep-space exposures.

14. SUBJECT TERMS
Radiation injury; Track structure; Nuclear fragmentation; Relative biological effectiveness

15. NUMBER OF PAGES
30

16. PRICE CODE
A03

17. SECURITY CLASSIFICATION OF REPORT	18. SECURITY CLASSIFICATION OF THIS PAGE	19. SECURITY CLASSIFICATION OF ABSTRACT	20. LIMITATION OF ABSTRACT
Unclassified	Unclassified		

NSN 7540-01-280-5500

Standard Form 298(Rev. 2-89)
Prescribed by ANSI Std. Z39-18
298-102

NASA-Langley, 1992